Eva Rajo-Iglesias
Departamento de Teoria de la Señal y Comunicaciones
University Carlos III of Madrid
Despacho 4.3B10
Avenida de la Universidad,
30, 28911 Leganés, Madrid, Spain
Tel: +34 91 624 8774;
Fax: +34 91 624 8749
E-mail: eva@tsc.uc3m.es

A Review of Implantable Patch Antennas for Biomedical Telemetry: Challenges and Solutions

Asimina Kiourti and Konstantina S. Nikita

BIOSIM Laboratory, Faculty of Electrical and Computer Engineering
National Technical University of Athens
9, Iroon Polytechniou Str., 15780 Zografos, Athens, Greece
Tel: +30 - 210 - 7722968; Fax: +30 - 210 - 7722320
E-mail: akiourti@biosim.ntua.gr, knikita@ece.ntua.gr

Abstract

Biomedical telemetry permits the transmission (telemetering) of physiological signals at a distance. One of its latest developments is in the field of implantable medical devices (IMDs). Patch antennas currently are receiving significant scientific interest for integration into the implantable medical devices and radio-frequency (RF)-enabled biotelemetry, because of their high flexibility in design, conformability, and shape. The design of implantable patch antennas has gained considerable attention for dealing with issues related to biocompatibility, miniaturization, patient safety, improved quality of communication with exterior monitoring/control equipment, and insensitivity to detuning. Numerical and experimental investigations for implantable patch antennas are also highly intriguing. The objective of this paper is to provide an overview of these challenges, and discuss the ways in which they have been dealt with so far in the literature.

Keywords: Biocompatible antenna; implantable antenna; industrial scientific and medical (ISM) band; medical implant communications service (MICS) band; medical telemetry; electrically small antenna; patch antenna; phantom; specific absorption rate (SAR)

1. Introduction

Biomedical telemetry permits the measurement of physiological signals at a distance, through either wired or wireless communication technologies. Physiological signals are obtained by means of appropriate transducers, post-processed, and eventually transmitted to exterior monitoring/control equipment. One of the latest developments of biomedical telemetry is in the field of implantable medical devices (IMDs) [1]. Low-frequency inductive links have long been the most prevalent method of biotelemetry for implantable medical devices [2, 3]. However, they suffer from low data rates (1-30 kbps), restricted range of communication (<10 cm), and increased sensitivity to inter-coil positioning. To overcome these limitations, research is currently oriented towards radio-frequency (RF)-linked implantable medical devices.

Millions of people worldwide depend upon implantable medical devices to support and improve the quality of their lives. RF-linked implantable medical devices are already in use for a wide variety of applications, including temperature monitors [4], pacemakers and cardioverter defibrillators [5], functional electrical stimulators (FES) [6], blood-glucose sensors [7], and cochlear [8] and retinal [9] implants. As technology continues to evolve, new implantable medical devices are being developed, and their use is expected to rapidly increase from an already large base.

Until recently, no globally accepted frequency band had been dedicated to biotelemetry for implantable medical devices. The situation changed with the ITU-R Recommendation SA.1346 [10], which outlined the use of the 402.0-405.0 MHz frequency band for Medical Implant Communications Systems (MICS). The spectrum of 3 MHz allows for 10 channels (a bandwidth of 300 KHz each) in order to support simultaneous operation of multiple implantable medical devices in the same area, and to limit interference from the co-located Meteorological Aids Service band (401-406 MHz). The MICS band is currently regulated by the United States Federal Communications Commission (FCC) [11] and the European Radiocommunications Committee (ERC) [12]. The 433.1-434.8 MHz, 868-868.6 MHz, 902.8-928 MHz, and 2400-2500 MHz Industrial, Scientific, and Medical (ISM) bands are also suggested for implantable medical device biotelemetry in some countries [13]. However, focus is on the MICS band, because of its advantages of being available worldwide and being feasible with low-power and low-cost circuits, reliably supporting high-data-rate transmissions, falling within a relatively low-noise portion of the spectrum, lending itself to small antenna designs, and acceptably propagating through human tissue. A review of the regulatory standards for implantable medical devices and the characteristics of MICS transceivers was performed in [14].

A key and critical component of RF-linked implantable medical devices is the integrated implantable antenna, which enables bidirectional communication with the exterior monitoring/control equipment. Patch designs are currently receiving considerable attention for implantable antennas, because they are highly flexible in design, shape, and conformability [15-17], thus allowing for relatively easy miniaturization and integration into the shape of the implantable medical device. In a realistic scenario, implantable patch antennas will be mounted on the existing hardware of the implantable medical device, which will also serve as the ground plane.

The design of implantable patch antennas has attracted high scientific interest for fulfilling the requirements of biocompatibility, miniaturization, patient safety, and high-quality communication with exterior equipment. Numerical and experimental investigations are also highly intriguing. An overview of these challenges is hereafter presented, and ways in which they have been dealt with so far in the literature are discussed.

2. Design

The requirements and constraints related to the design of implantable patch antennas are as follows.

2.1 Biocompatibility

Implantable antennas must be biocompatible in order to preserve patient safety and prevent rejection of the implant. Furthermore, human tissues are conductive, and would short-circuit the implantable antenna if they were allowed to be in direct contact with its metallization. Biocompatibility and prevention of undesirable short-circuits are especially crucial in the case of antennas that are intended for long-term implantation.

The most widely used approach for preserving the biocompatibility of the antenna – while at the same time separating the metal radiator from human tissue – is to cover the structure with a superstrate dielectric layer (e.g., Figure 1a [18]). Commonly used biocompatible materials include Teflon (permittivity, $\varepsilon_r = 2.1$; dielectric loss tangent, $\tan\delta = 0.001$), MACOR® ($\varepsilon_r = 6.1$; $\tan\delta = 0.005$), and ceramic alumina ($\varepsilon_r = 9.4$; $\tan\delta = 0.006$) [15]. However, it is important to highlight that ceramic substrates do not easily lend themselves to drilling and round cuts [19].

Insulating the implantable antenna with a thin layer of low-loss biocompatible coating is another reported approach (e.g., Figure 1b [20]). Materials proposed for biocompatible encapsulation include zirconia ($\varepsilon_r = 29$; $\tan\delta \approx 0$) [21], PEEK ($\varepsilon_r = 3.2$; $\tan\delta = 0.01$) [22], and Silastic MDX-4210 Biomedical-Grade Base Elastomer ($\varepsilon_r = 3.3$; $\tan\delta \approx 0$) [20]. Because of its electrical properties, zirconia is a better candidate material for biocompatible insulation from an electromagnetic point of view. High permittivity and low loss-tangent values allow the near fields of the antenna to concentrate inside the low-loss encapsulation layer, thus mitigating power loss. However, PEEK and Silastic MDX-4210 Biomedical-Grade

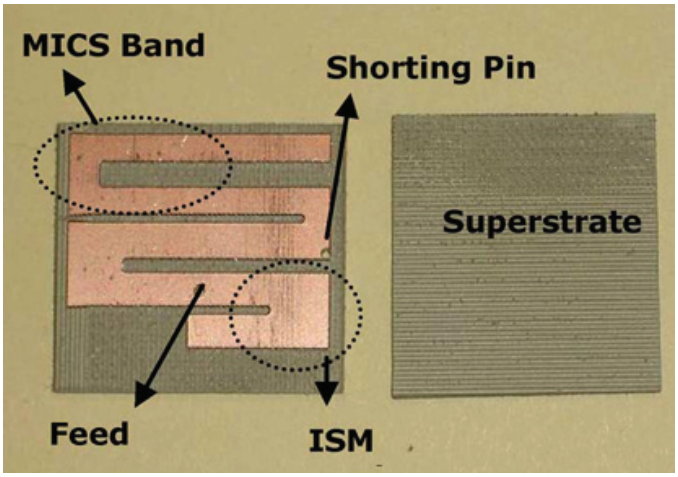

Figure 1a. Biocompatibility issues for implantable patch antennas: the addition of a superstrate [18].

Figure 1b. Biocompatibility issues for implantable patch antennas: thin-layer encapsulation [20].

Base Elastomer are much easier to prepare and handle. The thickness of the biocompatible insulation layer is an important factor in antenna design. The computation of its optimum value is considered to be highly significant for lowering power loss without aimlessly increasing antenna size [21, 22].

2.2 Miniaturization

Recent advances in the technology of implantable-medical-device electronics have led to ultra-small designs for implantable medical devices. For example, retinal prosthesis implantable medical devices are small enough to be inserted inside the eyeball (a radius of ~12.5 mm). The dimensions of the traditional half-wavelength ($\lambda/2$) or quarter-wavelength ($\lambda/4$) antennas at the frequency bands allocated for medical implants – and especially at the low-frequency MICS band – make them useless for implantable applications. Therefore, miniaturization becomes one of the greatest challenges in implantable-antenna design.

Human tissue in which implantable antennas are intended to operate exhibits relatively high permittivity (e.g., the relative permittivity of skin tissue at 402 MHz is 46.7 [23-25]), or, equivalently, reduced wave-propagation velocity, which, in turn, work to advantageously miniaturize the physical size of the antenna. However, it should be noted that when a low-permittivity biocompatible layer is inserted around the antenna, the value of the effective permittivity decreases, and miniaturization achieved by the high-permittivity tissue material is degraded.

The use of patch designs for implantable antennas allows for several additional miniaturization techniques. The aim is to reduce the size of the antenna at a given operating frequency, while still maintaining adequate electromagnetic performance. Miniaturization techniques proposed in the literature for implantable patch antennas include:

1. The use of high-permittivity dielectric (substrate/superstrate) materials: high-permittivity dielectrics are selected for implantable patch antennas (e.g., ceramic alumina, $\varepsilon_r = 9.4$ [26] or Rogers 3210, $\varepsilon_r = 10.2$ [27]) because they shorten the effective wavelength and result in lower resonance frequencies, thus assisting in antenna miniaturization. However, even with such high-permittivity dielectrics, the superstrate layer still insulates the antenna from the higher-permittivity tissue. Thicker superstrates increase the operating frequency of the antenna, and, in turn, require enhanced physical dimensions to refine resonance [28]. Dielectric materials with high permittivity values and thin superstrate layers are thus solicited.

2. Lengthening of the current-flow path on the patch surface: longer effective current-flow paths excited on the radiating patch can reduce the resonance frequency, and achieve a more-compact size for the implantable antenna. For this purpose, meandered [29], spiral [29], waffle-type [30], and hook-slotted [31] shaped patches have been suggested, as shown in Figure 2.

3. The addition of shorting pins: inserting a shorting pin between the ground and patch planes increases the effective size of the antenna, and, in turn, reduces the required physical dimensions, given a specific operating-frequency scenario. The technique works in much the same way that a ground plane doubles the height of a monopole antenna, i.e., it typically produces a planar inverted-F antenna (PIFA) with the same resonance performance as a double-sized antenna without the shorting pin [15].

4. Patch-stacking: vertically stacking two radiating patches reduces antenna size by increasing (nearly doubling) the length of the current-flow path [26, 27].

Implantable antennas reported in the literature combine some (or all) of these miniaturization techniques in order to reduce size. All antenna design parameters, including the location of the coaxial feed, have to be appropriately selected (optimized) for a good 50-ohm match at the desired operating

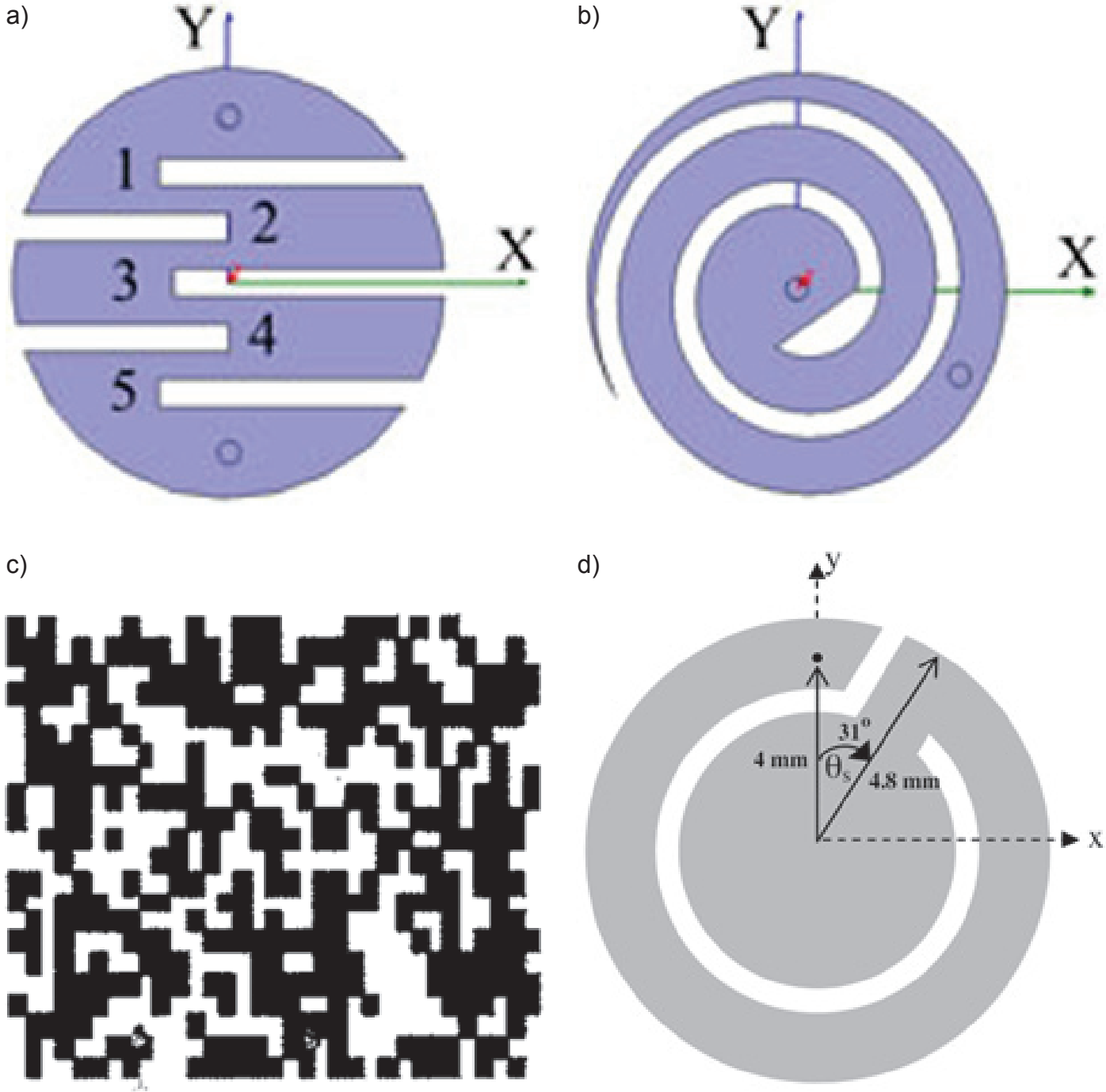

Figure 2. Lengthening of the current-flow path on the patch surface: (a) meandered [29], (b) spiral [29], (c) waffle-type [30], and (d) hook-slotted [31] shaped patches.

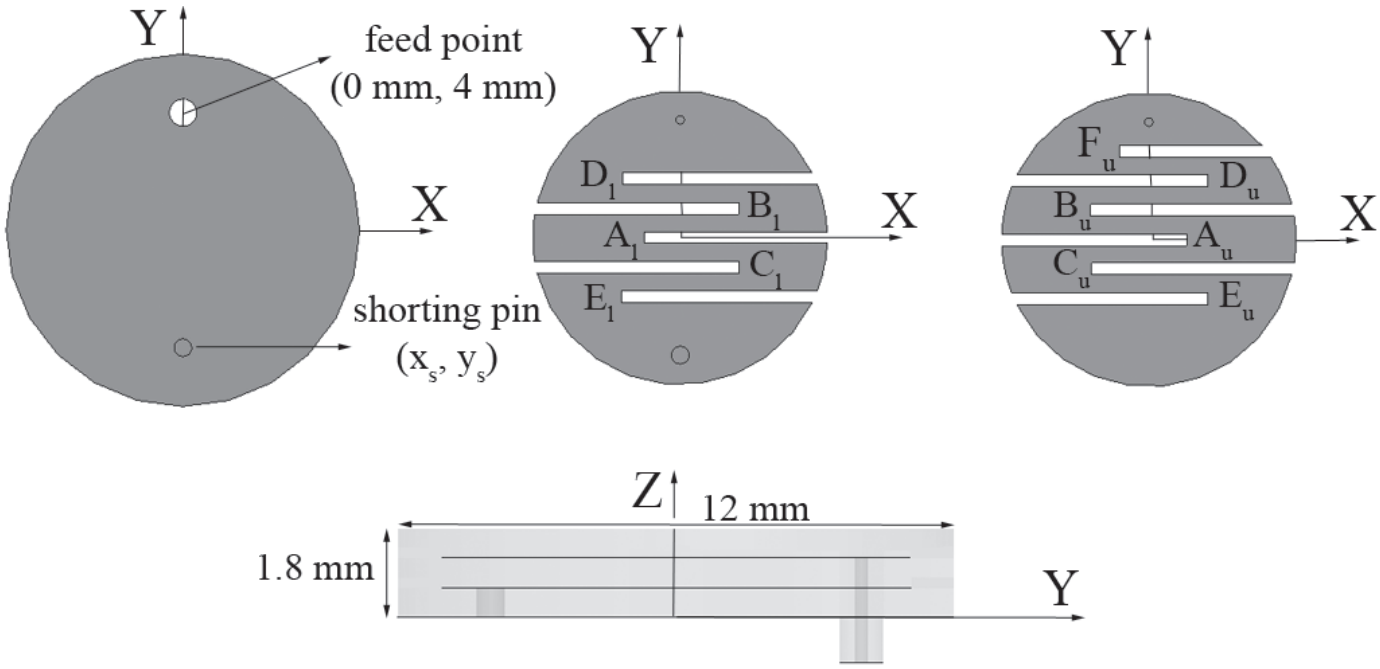

Figure 3. The geometry of a stacked skin-implantable PIFA with meandered patches [27].

frequency. For example, the skin-implantable antenna of Figure 3 adapted a stacked PIFA structure of meandered patches built on Rogers 3210 substrate to achieve a miniaturized structure (a volume of $214.9\ \text{mm}^3$), resonating in the MICS band [27].

Table 1 compares the volume occupied by MICS implantable-patch antennas reported in the literature with respect to the applied miniaturization techniques [15, 18, 26-28, 30-42]. The bands of operation covered, as well as the shapes of the antennas, are also included. When the number of bands of operation is increased, the size of the antenna is typically increased to cover them. A circular shape is generally preferred, in order to avoid sharp edges that could cause injury.

2.3 Patient Safety

Issues related to patient safety limit the maximum allowable power incident on the implantable antenna. The Specific Absorption Rate (SAR) (the rate of energy deposited per unit mass of tissue) is generally accepted as the most appropriate dosimetric measure, and compliance with international guidelines is assessed. For example, the IEEE C95.1-1999 standard restricts the SAR averaged over any 1 g of tissue in the shape of a cube to less than 1.6 W/kg ($\text{SAR}_{1g,max} \le 1.6$ W/kg) [43]. The ICNIRP basic restrictions limit the SAR averaged over 10 g of contiguous tissue to less than 2 W/kg [44]. To harmonize with the ICNIRP guidelines, the IEEE C95.1-2005 standard restricts the SAR averaged over any 10 g of tissue in the shape of a cube to less than 2 W/kg ($\text{SAR}_{10g,max} \le 2$ W/kg) [45].

The power absorbed by the human body in the presence of an incident electromagnetic field is given by

$$P_{abs} = \frac{1}{2}\int \sigma |E|^2 \, dV \,, \qquad (1)$$

where σ is the conductivity of the human tissues, and $|E|$ is the intensity of the electric field inside the body [32]. Equation (1) indicates that the absorbed power is related to the electric field, so that maximum SAR values are recorded in the areas where maximum electric-field intensities occur. Based on the deduction that peak averaged SAR values are generated from high near fields, novel implantable patch antennas can be designed that aim at lower electric-field intensities.

The radiation mechanism of an implantable antenna was discussed in [34] in an attempt to modify its design for reducing the spatially averaged SAR in human tissue. Replacing the uniform-width spiral radiator of an implantable MICS PIFA with a nonuniform-width radiator was found to decrease the electric-field intensity and, in turn, the $\text{SAR}_{1g,max}$. The simulated near-electric-field distribution showed that the high electric-field area of the PIFA employing the nonuniform-width radiator (Figure 4a) was much smaller than that of the original PIFA (Figure 4b). The value of $\text{SAR}_{1g,max}$ was thus reduced from 310 W/kg to 210 W/kg, considering a net input power of 1 W.

Table 2 compares the computed $\text{SAR}_{1g,max}$ and $\text{SAR}_{10g,max}$ values for the MICS implantable patch antennas of Table 1 (where available) [15, 18, 26-28, 30-42]. Maximum

Table 1. A comparison of the volume occupied by MICS implantable patch antennas reported in the literature, with respect to the miniaturization techniques employed.

Ref	Substrate Shape	Implantation Tissue	Bands [MHz]	Miniaturization Technique				Vol. [mm^3]
				Dielectric Material	Patch Shape	Shorting Pin	Patch Stacking	
[32]	rectangular	skin	402-405	Rogers 3210 (1)	spiral	–	–	10240.0
[30]	rectangular	2/3 muscle	402-405	RT/duroid 6002 (2)	waffle	yes	–	6480.0
[32]	rectangular	skin	402-405	Rogers 3210 (1)	spiral	yes	–	6144.0
[15]	rectangular	2/3 muscle	402-405	MACOR® (3)	spiral	yes	–	3457.4
[33]	square	skin	402-405 2400-2480	ARLON1000(4)	SRR coupled to a spiral	yes	–	1375.4*
[18]	rectangular	skin	402-405 2400-2480	Rogers 3210 (1)	meandered	yes	–	1265.6
[34]	rectangular	skin	402-405	Rogers 3210 (1)	spiral	yes	–	1200.0
[35]	rectangular	skin	402-405	Rogers 3210 (1)	meandered	yes	–	1200.0
[36]	rectangular	2/3 muscle	402-405	RT/duroid 6010 (5)	spiral	yes	–	823.0
[37]	rectangular	muscle	402-405	Rogers 3210 (1)	π-shaped	yes	–	790.9
[38]	circular	skin	402-405	Rogers 3210 (1)	hook-slotted	yes	yes	335.8
[39]	square	vitreous humor	402-405	Rogers 3210 (1)	spiral	yes	yes	273.6
[40]	square	skin	402-405 433-435 2400-2480	Rogers 3210 (1)	comb and π-shaped	yes	yes	254.0
[27]	circular	skin	402-405	Rogers 3210 (1)	meandered	yes	yes	203.6
[41]	square	skin	402-405	Rogers 3210 (1)	spiral	yes	yes	190.0
[31]	circular	skin	402-405	Rogers 3210 (1)	hook-slotted	yes	yes	149.2
[42]	square	skin	402-405	Rogers 3210 (1)	hook-slotted	yes	yes	121.6
[28]	circular	skin	402-405	Rogers 3210 (1)	meandered	yes	yes	110.4
[26]	circular	skin	402-405	alumina (6)	meandered	yes	yes	32.7

(1) $\varepsilon_r = 10.2$, (2) $\varepsilon_r = 2.94$, (3) $\varepsilon_r = 6.1$, (4) $\varepsilon_r = 6.1$, (5) $\varepsilon_r = 10.2$, (6) $\varepsilon_r = 9.4$; * O. Quevedo-Teruel, personal communication

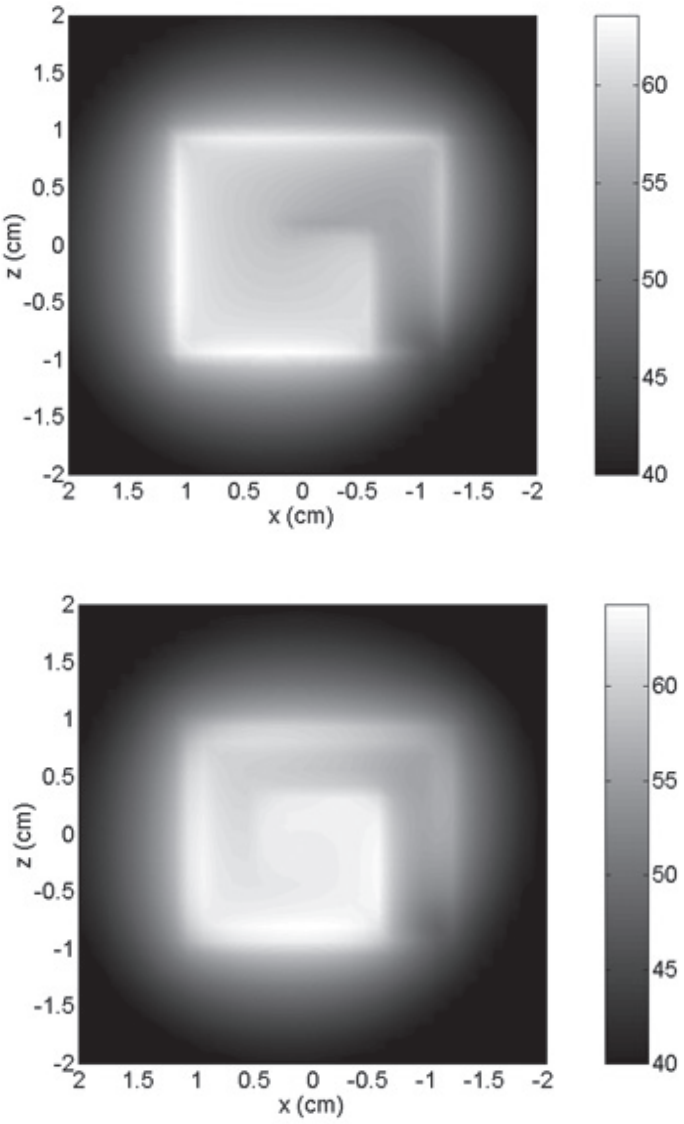

Figure 4. The near electric field distribution in front of (a, top) nonuniform-width and (b, bottom) uniform-width radiators of a spiral implantable patch antenna [34].

allowable net-input-power levels to the antennas are also shown, as restricted by the IEEE C95.1-1999 ($P_{C95.1\text{-}1999}$) [43] and IEEE C95.1-2005 ($P_{C95.1\text{-}2005}$) [45] standards. Increased-size implantable antennas exhibit more uniform distributions of the electric field and current density across an increased patch surface area, so that lower SAR values are obtained. The IEEE C95.1-1999 [43] standard appears to be much stricter than the IEEE C95.1-2005 [45] standard.

2.4 Far-Field Gain

Medical implant communication systems (MICS) are comprised of the implantable medical device and an exterior monitoring/control device, which is placed at some distance (typically, 2 m) away from the body [10]. Biotelemetry links may be used for device-parameter adjustment, transmission of stored information, as well as real-time transmission of vital monitoring information. The implantable antenna should thus provide a signal that is strong enough to be picked up by the exterior device, regardless of any power limitations. It is important to highlight that apart from patient safety, interference issues also limit the maximum allowable power incident on the implantable antenna. For example, a strict limit of −16 dBm (25 μW) has been set on the effective radiated power (ERP) of implantable medical devices operating in the MICS band, in order to prevent interference to the collocated Meteorological Aids Service band [10].

Given the SAR and effective radiated power limitations, the far-field gain of the implantable antenna indicates the desired receiver sensitivity for achieving reliable biotelemetry communication. In order to increase the range of biotelemetry communication, implantable antennas with enhanced gain are solicited. However, reduced-size antennas exhibit degraded electromagnetic performance: miniaturization degrades gain, while high-gain antennas exhibit relatively increased size. The maximum far-field gain values (G_{max}) achieved by the MICS implantable antennas of Table 1 are shown in Table 2 (where available). Low values of gain imply poor radiation efficiencies; however, compromises in the system's performance are inevitable, given the miniaturized antenna dimensions.

(A)symmetry of the implantation tissue model affects symmetry of the antenna's far-field radiation pattern, accordingly. Omnidirectional, monopole-like radiation is observed inside symmetrical tissue models (e.g., Figure 5a [26, 27]), whereas asymmetrical radiation is recorded within anatomical tissue models that are irregular and inhomogeneous (e.g., Figure 5b [26, 27]).

2.5 Low Power Consumption

If operated continuously, the implantable medical device's transceiver will consume significant energy, and reduce the lifetime of the implantable medical device. There exist some methods for recharging the battery (e.g., via an inductive-loop approach [2, 3]). However, using the biotelemetry link only when necessary would be highly advantageous.

For this purpose, a transceiver with dual-band operation may be used, such as the commercially available Zarlink ZL70101 transceiver [46]. The system uses two frequency bands, one for "wake-up" and one for transmission. The transceiver stays in "sleep mode" with low power consumption (1 μW) until a "wake-up" signal is sensed in the 2450 MHz ISM band. In the normal mode, the implantable medical device is fully powered, and exchanges data in the MICS band. Following the data transfer, the implantable medical device's transceiver returns back to the "sleep mode." The exterior device may be programmed to wake up the implanted device according to a physician-defined schedule, or only when a patient event is detected [14].

For example, a dual-band (MICS and ISM) implantable antenna was proposed in the literature for continuous glucose

Table 2. A performance comparison of MICS implantable patch antennas reported in the literature with respect to the occupied volume: maximum 1 g ($SAR_{1g,max}$) and 10 g ($SAR_{10g,max}$) averaged SAR for a net input power of 1 W, with maximum allowable net-input-power levels imposed by the IEEE C95.1-1999 ($P_{C95.1\text{-}1999}$) and IEEE C95.1-2005 ($P_{C95.1\text{-}2005}$) standards, maximum far-field gain (G_{max}), and bandwidth at a return loss of 10 dB (10 dB-BW) (where available).

Ref.	Volume [mm^3]	$SAR_{1g,max}$ [W/kg]	$SAR_{10g,max}$ [W/kg]	$P_{C95.1\text{-}1999}$ [mW]	$P_{C95.1\text{-}2005}$ [mW]	G_{max} [dB]	10 dB-BW [MHz]
[32]	10240.0	182.0	–	8.791	–	–	20
[30]	6480.0	–	–	–	–	–	16
[32]	6144.0	209.0	–	7.656	–	–	25
[15]	3457.4	–	–	–	–	–	28
[33]	1524.0*	–	–	–	–	–6*	12*
[18]	1265.6	–	–	–	–	–25	142
[34]	1200.0	310.0	–	5.161	–	–	28
[35]	1200.0	294.0	–	5.442	–	–	40
[36]	823.0	274.9	–	5.820	–	–	25
[37]	790.9	280.0	–	5.714	–	–27	120
[38]	335.8	333.5	–	4.798	–	–26	50
[39]	273.6	–	–	–	–	–24	39
[40]	254.0	341.0	–	4.692	–	–7	113
[27]	203.6	324.7	66.6	4.928	30.030	–37	27
[41]	190.0	336.0	–	4.762	–	–26	50
[31]	149.2	716.0	–	2.235	–	–	84
[42]	121.6	900.0	–	1.778	–	–38	122
[28]	110.4	828.3	96.6	1.932	20.704	–46	50
[26]	32.7	679.8	82.0	2.354	24.390	–45	40

* O. Quevedo-Teruel, personal communication

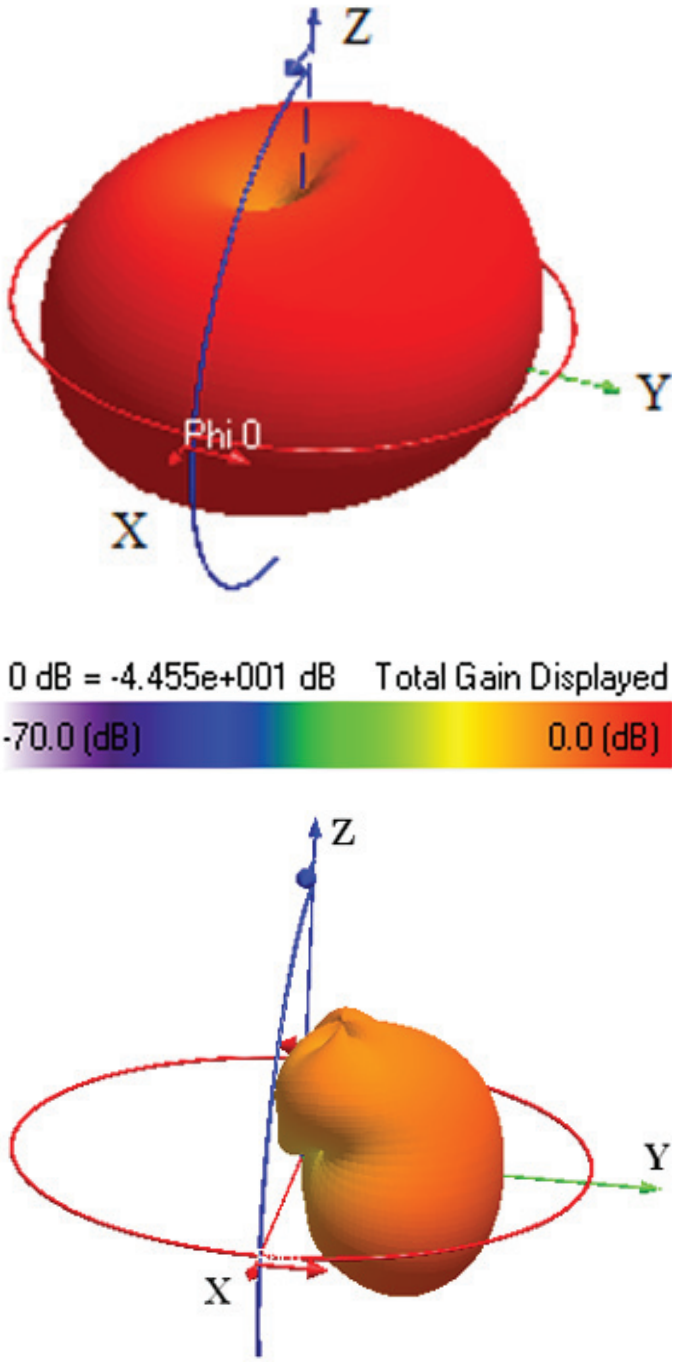

Figure 5. The far-field-gain radiation patterns of the skin-implantable antenna proposed in [26] inside (a, top) a 100 mm-edge skin cube, and (b, bottom) the skin tissue of an anatomical human head model.

monitoring [18]. A meandered antenna configuration was considered for optimizing the antenna's surface area, and particle-swarm optimization was applied to achieve the desired resonance characteristics. The simulated and measured bandwidths were found to be 82 MHz and 142 MHz in the MICS band, and 103 MHz and 174 MHz in the ISM band, respectively. An innovative dual-band (MICS and ISM) patch antenna with a multilayer configuration and electromagnetic-coupling-based feeding was further proposed for implantation inside the left sub-pectoral region [33]. Recently, a novel antenna design was suggested using a π-shaped radiator with stacked and spiral structure to support triple-band operation with data telemetry (402 MHz), wireless power transmission (433 MHz), and wake-up controller (2450 MHz) [40]. The simulated and measured bandwidths were 86 MHz and 114 MHz in the MICS band, and 60 MHz and 70 MHz in the ISM band, respectively.

3. Numerical Investigations

3.1 Tissue Models

In numerical simulations, implantable antennas are analyzed inside inhomogeneous lossy media that simulate biological tissues. Biological tissues have their own permittivity (ε_r), conductivity (σ), and mass-density values. Canonical tissue models are often used to speed up simulations, and to ease the design of implantable antennas. These may be a single layer (e.g., Figure 6a [27]), thus accounting for a generic tissue-implantable antenna. They may also be multilayer (e.g., Figure 6b [18]), thus providing a simplified model of a specific implantation site inside the human body. Example canonical tissue models used in the literature for the simulation of implantable patch antennas are shown in Table 3 [15, 18, 26-32, 34, 35, 41, 42].

To obtain more realistic results, anatomical tissue models (e.g., Figure 6c [27]), produced by the combination of magnetic-resonance imaging (MRI) or computer tomography (CT) data with the electrical properties of human body tissues, can also be applied. Anatomical tissue models used in the literature for simulation of implantable patch antennas are shown in Table 4 [15, 26, 27, 29, 32].

As far as antenna design is concerned, it is important to highlight that multilayer canonical models have been

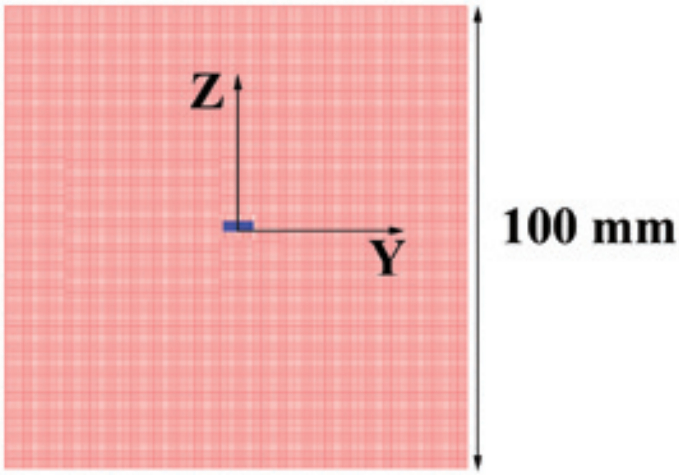

Figure 6a. A single-layer canonical (skin cube) tissue model [27].

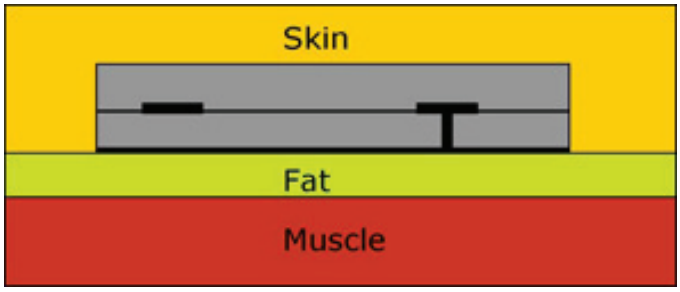

Figure 6b. A three-layer (skin/fat/muscle) canonical tissue model [18].

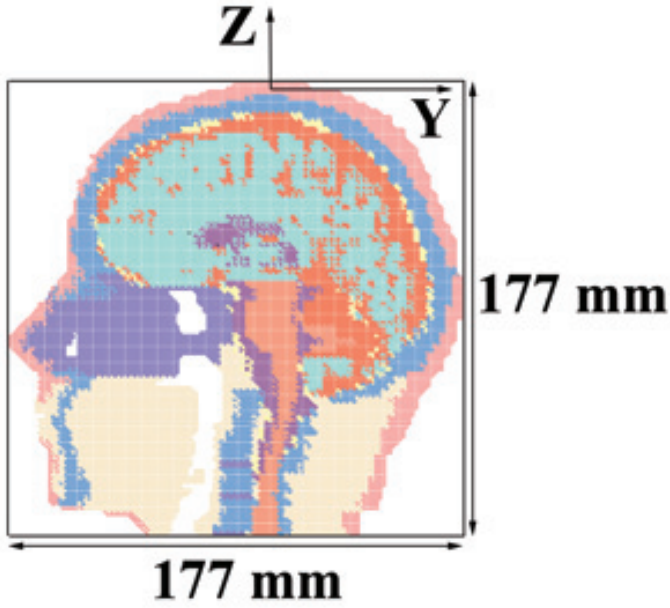

Figure 6c. An anatomical human head tissue model [27].

proven to provide an acceptable model for the human body. Highly similar return-loss characteristics have been found for implantable patch antennas inside a three-layer planar geometry and a realistic model of the human chest [32], as well as inside a three-layer spherical and an anatomical model of the human head [27].

3.2 Numerical Methods and Software

Analytical methods can only be applied for analyzing the performance of simplified implantable antennas positioned inside canonical tissue models. For example, a spherical dyadic Green's function (DGF) code was implemented in the literature to characterize a MICS dipole antenna implanted inside a multilayer spherical human-head model [32]. As a result, emphasis is mainly on numerical methods implemented on commercial electromagnetic simulation platforms.

The electromagnetic solvers that are most commonly used in the literature for implantable antenna design are based on the Finite-Element (FE) Method (e.g., Ansoft *HFSS*) [28, 31, 36, 41]. The Finite-Difference Time-Domain (FDTD) Method is also applied in some studies, because it exhibits simplicity in the implementation of inhomogeneous media and assessment of bioelectromagnetic interactions, while enabling efficient modeling of detailed anatomical human body parts (e.g., CST *Microwave Studio*, Remcom *XFDTD*) [15, 26-28, 32, 34]. In all cases, the computational cost heavily depends on the complexity of the tissue and antenna models.

The frequency dependency of tissue dielectric values (ε_r , σ) is taken into account by using Cole-Cole models [18], or simpler two-pole Debye models [47], which can be efficiently incorporated into numerical codes. Absorbing boundaries (e.g., Mur [15] or perfectly matched layer boundaries [30]) are placed at some distance away from the setups to truncate the simulation domain while extending radiation infinitely far.

3.3 Antenna Design Strategies

Several strategies have been proposed for implantable antenna design. These are mainly dictated by the fact that antennas are intended to operate inside human tissue instead of free space. The antenna should therefore be designed inside free space, and further refined for tissue implantation, or designed directly inside an environment surrounded with human tissue.

In [48], a MICS patch antenna was designed in a free-space environment, and further implanted inside the skin tissue

Table 3. Canonical tissue models used in the literature for analysis of implantable patch antennas.

Canonical Tissue Model			Ref.
Body Part	**Tissue(s)**	**Shape (volume [mm^3])**	
Generic skin	skin	cubic (100 × 100 × 100)	[26-29]
		rectangular (16 × inf × inf)	[32]
		rectangular (8.5 × 102.5 × inf)	[18]
		rectangular (50 × 100 × 100)	[31] [34] [35]
		cylindrical ($\pi \times (10)^2 \times 20$)	[41] [42]
Average body	2/3 muscle	rectangular (20 × 40 × 50)	[15]
		rectangular (20 × 50 × 60)	[30]
Head	skin/bone/brain	spherical ($\pi \times (100)^3$)	[27]
	skin/fat/bone/ dura/CSF/brain	spherical ($\pi \times (90)^3$)	[32]
Left upper chest	skin/fat/muscle	rectangular (16 × inf × inf)	[32]

Table 4. Anatomical tissue models used in the literature for analysis of implantable patch antennas.

Anatomical Tissue Model			Ref.
Body Part	**# of Tissues**	**Max Dimensions [mm]**	
chest	30	286 × 320 × 584	[32]
shoulder	31	180 × 190 × 390	[15]
head	13	160 ×177 × 177	[26] [27] [29]
	30	200 × 256 × 280	[32]
head with shoulders	30	288 × 400 × 620	[32]

of an anatomical head model. Resonance-frequency detuning was observed, as attributed to the capacitive loading effect of the surrounding tissues, and a varactor diode with tuning capability was inserted to refine resonance.

In [22], a MICS antenna was designed in free space, aimed at high gain (higher than -20 dB), in order to account for subsequent body-absorption losses. The antenna was optimized in free space to minimize size, and further covered by a biocompatible layer and placed inside tissue material. Design modifications were performed to account for the frequency shift induced by the presence of encapsulation and human tissue.

Use of a single-layer tissue model is the simplest and fastest option when designing implantable antennas directly inside tissue material. Following this methodology, antennas are designed for a "generic" tissue-implantation scenario. Simplified tissue models in the shape of a cube [26-29], a rectangular parallelepiped [31-35] and a cylinder [41, 42] have been used for this purpose. The design is performed by selecting the dielectric material, and subsequently optimizing all antenna design parameters to refine tuning at the desired operating frequency.

Another option is to design the antenna for a specific implantation site by taking into account a specific region of the body. A multilayer tissue model, with either finite or infinite dimensions, is selected in this case. For example, implantable antennas intended for trunk [18] and chest [32] implantation were directly designed inside three-layer planar tissue models consisting of skin, fat, and muscle tissues.

Recently, a novel two-step design methodology was proposed for implantable antennas. This emphasizes design speed-up and optimized resonance performance inside a specific implantation site [27]. This involves an approximate antenna design inside a simplified tissue model (a cube filled with the intended tissue material), and further quasi-Newton optimization inside a canonical model of the desired implantation site. Despite being optimized inside a canonical tissue model, the designed antennas were shown to exhibit insignificant resonance discrepancies inside detailed anatomical tissue models.

4. Experimental Investigations

Experimental investigations are required in order to confirm the validity of numerical simulations for implantable antennas. Since it is not possible to carry out measurements inside real operating scenarios (i.e., inside the human body), investigations are performed by measuring laboratory-fabricated prototypes inside either tissue-equivalent mediums (phantoms) or animal tissue.

4.1 Prototype Fabrication

Due to the unavailability of biocompatible materials in some laboratories, other dielectrics with similar electrical properties may be selected for prototype fabrication. For instance, Rogers 3210 ($\varepsilon_r = 10.2$, $\tan\delta = 0.003$) is often used because it has properties similar to the biocompatible ceramic alumina ($\varepsilon_r = 9.4$, $\tan\delta = 0.006$) [18, 27, 31].

Prototype fabrication of implantable antennas meets all classical difficulties of miniature antennas. For example, additional glue layers used to affix all components together strongly affect antenna performance, by shifting the antenna's resonance frequency and degrading its matching characteristics [22, 27]. Furthermore, the coaxial cable feed used to connect the antenna with the network analyzer may give rise to radiating currents on the outer part of the cable, which, in turn, deteriorate measurements. The effects of different feeding techniques for implantable patch antennas were analyzed in [49]. Patch-antenna prototypes immersed inside phantoms, with the ground plane being in direct contact with the tissue-emulating material, were found to be insignificantly influenced by the coaxial feeding cable.

Based on the above, the numerical antenna model must be slightly adjusted in order to take prototype fabrication considerations into account. Example fabricated prototypes of implantable patch antennas are shown in Figure 7 [27, 36, 50]. Numerical simulations and experimental measurements must be carried out with the exact same antenna structure in order to be able to validate the design.

4.2 Testing Inside Phantoms

Testing inside phantoms is relatively easy and practical to implement. The fabricated prototype is immersed inside a tissue phantom (i.e., a container filled with a liquid or gel material that mimics the electrical properties of biological tissue), and measured. For validation purposes, the same scenario as that of the numerical simulations has to be considered.

Canonically-shaped phantoms have so far been used for testing of implantable patch antennas (e.g., Figure 8a [27]). In this case, the main challenge lies in the formulation and characterization of tissue-emulating materials. Example phantoms and tissue recipes reported in the literature are given in Table 5 [15, 18, 19, 27, 31, 32, 35, 36, 50, 51]. Recipes proposed mainly included deionized water, sugar, and salt. An increase in sugar concentration has been found to significantly decrease ε_r while slightly increasing σ. An increase in salt concentration decreases ε_r and significantly increases σ [18]. Adding gelatin or dry agarose to solidify the liquids and form multilayer gel phantoms was also examined (e.g., Figure 8b) [18, 51]. To

Figure 7a. A fabricated prototype of an implantable patch antenna [27].

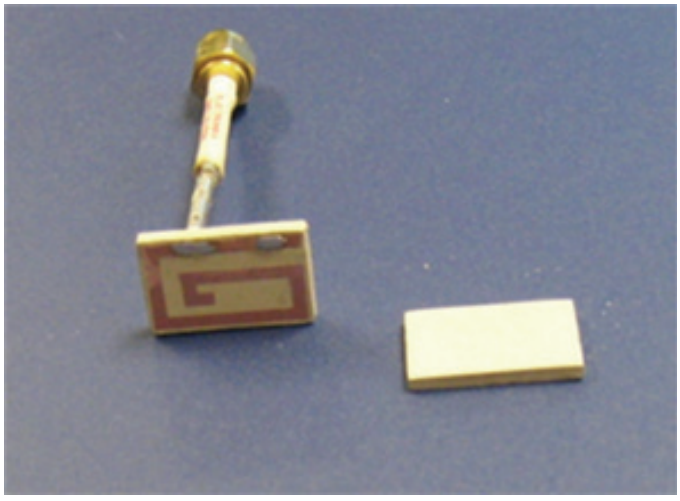

Figure 7b. A fabricated prototype of an implantable patch antenna [36].

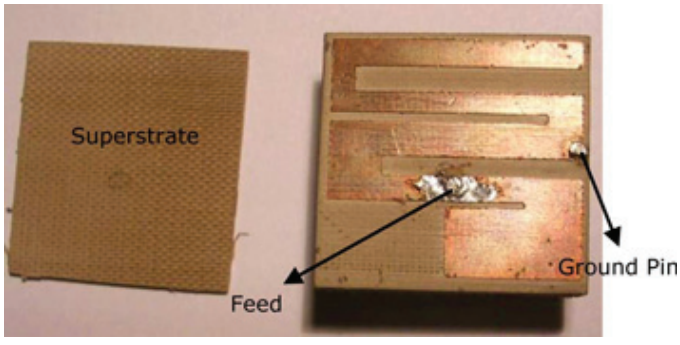

Figure 7c. A fabricated prototype of an implantable patch antenna [50].

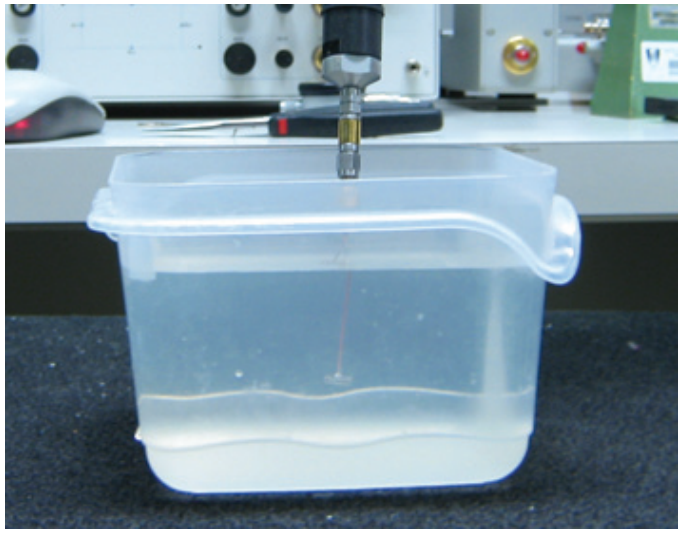

Figure 8a. A liquid canonical phantom used for testing of implantable patch antennas [27].

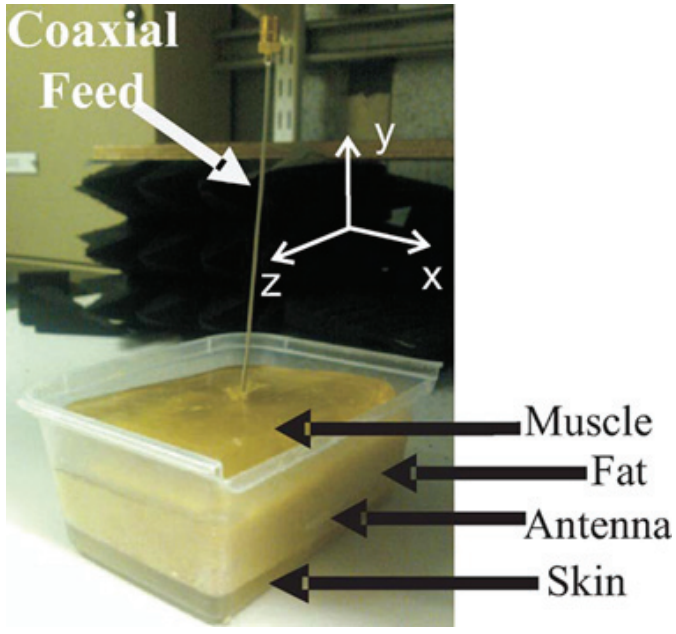

Figure 8b. A multilayer gel canonical phantom used for testing of implantable patch antennas [51].

Table 5. Phantoms used in the literature for testing of implantable patch antennas.

Phantom				Measured Electrical Properties			Ref
Tissue(s)	**Shape (volume [mm^3])**	**State**	**Ingredients**	f **[MHz]**	ε_r	σ **[S/m]**	
Skin	cubic (100 × 100 × 100)	liquid	deionized water, sugar, salt,	402	46.7	0.69	[27]
	rectangular (height of 100 mm)	liquid	deionized water / sugar / salt / cellulose	402	49.6	0.51	[32]
	rectangular (100 × 100 × 50)	liquid	deionized water, fruit sugar, salt, cellulose,	402	46.7	0.69	[31]
	rectangular (height of 50 mm)	liquid	–	402	49.6	0.51	[35]
	rectangular	gel	deionized water, sugar, salt, agarose	402	46.7	0.69	[18]
	rectangular	gel	deionized water, sugar, agarose	2450	38.1	2.27	[18]
2/3 muscle	rectangular	liquid	water sugar, salt, TX-151 powder,	402	48.9	0.71	[15]
	rectangular	liquid	water, sugar, salt, cellulose cetylpyridinium chloride	403	41.3	–	[36]
Scalp	rectangular	gel	water, salt, acrylamide, TMEDA, ammonium persulphate,	2450	50	2.2	[19]
Rat tissue	rectangular	gel	deionized water, salt, DGBE	402	0.78	1.3	[50]
	rectangular	gel	deionized water, DGBE, Triton X-100	2450	0.73	1.27	[50]
Skin Fat Muscle	rectangular (40 × 80 × 160)	(multilayer) gel	deionized water, sugar deionized water, salt, vegetable oil, flour deionized water, sugar, salt	868	38.7 4.9 53.0	0.77 0.04 0.92	[51]

prevent the formation of air bubbles and/or gaps, the mixture must be carefully heated and stirred, and slowly poured inside the container of the phantom. Since it is not possible to produce a valid approximation to human tissue for a broad frequency spectrum using a single formula, separate recipes are given for different frequency bands [18]. Measurements of the liquid's electrical properties (ε_r and σ) are conducted by either the open-ended coaxial cable technique [52], or a dielectric probe kit (e.g., Agilent's 85070E dielectric probe kit).

Most studies of implantable patch antennas are limited to reflection-coefficient (S_{11}) measurements (e.g., [27, 30-36]). As part of the experimental setup, prototype antennas are connected to a network analyzer through a coaxial cable, immersed inside the tissue-emulating phantom, and measured. Only in [19] was the transmission coefficient (S_{21}) measured through a scalp phantom at the 2450 MHz ISM band. In this study, a 2450 MHz PIFA was implanted inside a gel scalp phantom for intracranial pressure monitoring, and a linearly polarized 2450 MHz chip antenna was used as the receiving (probing) antenna.

4.3 Testing Inside Animal Tissue

Testing inside animal tissue can be performed either by embedding the implantable antenna inside tissue samples from donor animals, or by surgically implanting the antenna inside live model animals (in-vivo testing). In the first case, electrical properties of the test tissue can be measured using a dielectric probe kit and a network analyzer.

The use of animal-tissue samples provides an easy approach to mimicking the frequency-dependency characteristics of the electrical properties of tissues. This can prove highly advantageous when carrying out measurements for multi-band implantable antennas. In the literature, an implantable patch antenna with dual resonances at 380 and 440 MHz was tested inside test tissue obtained by grinding the front leg of a pig [37]. The electrical properties of the adapted pork were found to be between those of human skin and muscle in the MICS band. A dual-band skin-implantable patch antenna operating in the MICS and 2450 MHz ISM bands was also tested in real animal skin [50]. Skin samples with dimensions of 50 mm × 50 mm × 5 mm were extracted from the dorsal area of three donor rats to cover the designed antenna, and measurements were performed within 30 minutes of euthanasia (Figure 9a). Finally, a triple-band implantable patch antenna was tested inside a minced front leg of a pig [40]. The electrical properties of the minced pork were measured, and found to correspond to those of human skin and muscle between 100 MHz and 3 GHz.

In-vivo investigations are also vital in order to investigate the effects of live tissue on the performance of implantable patch antennas, while providing valuable feedback for antenna design and analysis. Testing inside living animals is highly challenging. An in-vivo testing protocol needs to be developed before the experimental investigations. This needs to deal with the choice and number of animals, pre-surgical preparation, anesthesia, surgical procedure, measurements (e.g., repeatability requirements, determination of potential sources of noise), and post-surgical treatment. In-vivo studies reported in the literature are very limited. The return-loss frequency response of a skin-implantable antenna was measured using rats as model animals [20] (Figure 9b). In this study, the antenna was implanted by means of a surgical operation inside the dorsal midline of three rats (for validation purposes), and euthanasia was applied after the measurements (approximately 13-15 minutes after the surgery). Canine studies for trans-scalp evaluation of a scalp-implantable antenna at 2450 MHz were also presented [53]. Canine models were selected to ensure a large head size. An intra-cranial pressure-monitoring device with an integrated PIFA was fixed to the skull. The monitor was tested while the dog was still under anesthesia. After the measurements, the animal was allowed to emerge from anesthesia and taken to the recovery area.

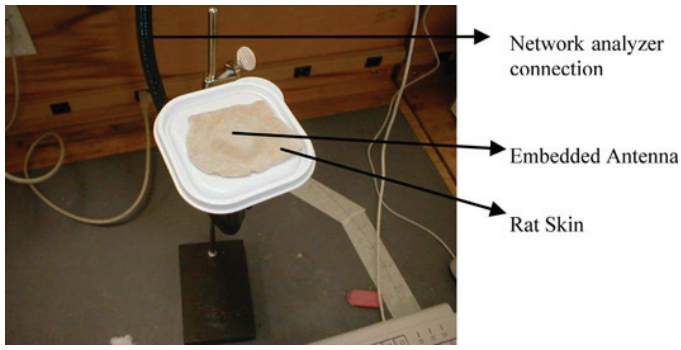

Figure 9a. The testing of an implantable patch antenna inside animal tissue: an antenna embedded inside rat-skin samples [50].

Figure 9b. The testing of an implantable patch antenna inside animal tissue: a antenna surgically implanted into a rat [20].

5. Conclusion

In this paper, we have presented an overview of the challenges faced and solutions suggested regarding the design, numerical simulations, and experimental investigations of implantable patch antennas for biomedical telemetry. The design of implantable antennas mainly emphasizes miniaturization issues and biocompatibility. However, electrically small antennas present poor radiation performance and relatively narrow bandwidths. Even though gain enhancement is considered crucial, compromises in the system performance are generally inevitable. Conserving energy to extend the lifetime of the implantable medical device is also significant. Multi-band antennas are being designed for this purpose that "wake up" the implantable medical device only when there is a need for information exchange.

The computational tools that are most commonly used for the numerical simulations of implantable patch antennas are based on the Finite-Element and Finite-Difference Time-Domain Methods. Several methodologies have been proposed for implantable antenna design, all of which need to take into account the host body. Simplified tissue models have proven to be able to substitute for complex anatomical tissue models, thus speeding up simulations. Although a homogenous model is sufficient for basic antenna design, a more-realistic model is needed to refine the final antenna design and provide accurate results. Using efficient and accurate simulation tools and tissue models is a key issue for both design and performance analysis.

Regarding experimental investigations, implantable antennas exhibit tight fabrication tolerances, attributed to their miniature size. Testing inside tissue-emulating phantoms mainly needs to deal with the formulation and characterization of the tissue-mimicking liquid or gel. To benefit from frequency-dependent tissue electrical properties, testing in animal tissue samples can additionally be performed. However, the highest challenge lies in measurements within living animals, for which careful consideration is required for developing the optimal testing protocol.

Implantable medical devices are a growing technology with a high potential for improving patients' life and the quality of healthcare. RF technology for implantable medical devices promises many benefits for both patients and caregivers. Even though emphasis has been given to implantable patch antennas, it is worth noting that the shape of the implantable medical device and the intended implantation site will actually dictate the type of the antenna. Patch antennas are appropriate for being integrated onto most flat implantable devices; however, a helical antenna might be more preferable for a urinary implant application.

6. References

1. W. Greatbatch and C. F. Homes, "History of Implantable Devices," *IEEE Engineering in Medicine and Biology Magazine*, **10**, 3, September 1991, pp. 38-41.

2. Z. Tang, B. Smith, J. H. Schild, and P. H. Peckham, "Data Transmission from an Implantable Biotelemeter by Load-Shift Keying Using Circuit Configuration Modulator," *IEEE Transactions on Biomedical Engineering*, **42**, 5, May 1995, pp. 524-528.

3. P. Valdastri, A. Menciassi, A. Arena, C. Caccamo, and P. Dario, "An Implantable Telemetry Platform System for In Vivo Monitoring of Physiological Parameters," *IEEE Transactions on Information Technology in Biomedicine*, **8**, 3, September 2004, pp. 271-278.

4. W. G. Scanlon, N. E. Evans, and Z. M. McCreesh, "RF Performance of a 418 MHz Radio Telemeter Packaged for Human Vaginal Placement," *IEEE Transactions on Biomedical Engineering*, **44**, 5, May 1997, pp. 427-430.

5. D. Wessels, "Implantable Pacemakers and Defibrillators: Device Overview and EMI Considerations," Proceedings of the IEEE International Symposium on Electromagnetic Compatibility (EMC 2002), August 2002.

6. K. Guillory and R. A. Normann, "A 100-Channel System for Real Time Detection and Storage of Extracellular Spike Waveforms," *Journal of Neuroscience Methods*, **91**, 1999 pp. 21-29.

7. M. C. Shults, R. K. Rhodes, S. J. Updike, B. J. Gilligan, and W. N. Reining, "A Telemetry-Instrumentation System for Monitoring Multiple Subcutaneously Implanted Glucose Sensors," *IEEE Transactions on Biomedical Engineering*, **41**, 10, October 1994, pp. 937-942.

8. T. Buchegger, G. Obberger, A. Reisenzahn, E. Hochmair, A. Stelzer, and A. Springer, "Ultra-Wideband Transceivers for Cochlear Implants," *EURASIP Journal on Applied Signal Processing*, **18**, 2005, pp. 3069-3075.

9. K. Gosalia, G. Lazzi, and M. Humayun, "Investigation of Microwave Data Telemetry Link for a Retinal Prosthesis," *IEEE Transactions on Microwave Theory and Techniques*, **52**, 8, August 2004, pp.1925-1932.

10. "International Telecommunications Union-Radiocommunications (ITU-R), Radio Regulations, SA.1346," ITU, Geneva, Switzerland; available online: http://itu.int/home.

11. "Medical Implant Communications Service (MICS) Federal Register," Rules Regulations, 64, 240, December 1999, pp. 69926-69934.

12. "European Radiocommunications Commission (ERC) Recommendation 70-03 Relating to the Use of Short Range Devices," European Conference of Postal and Telecommunications Administration, CEPT/ERC 70-03, Annex 12, 1997.

13. "International Telecommunications Union-Radiocommunications (ITU-R), Radio Regulations, Section 5.138 and 5.150," ITU, Geneva, Switzerland; available online: http://itu.int/home.

14. H. S. Savci, A. Sula, Z. Wang, N. S. Dogan, E. Arvas, "MICS Transceivers: Regulatory Standards and Applications," Proceedings of the IEEE International Southeast Conference, April 2005.

15. P. Soontornpipit, C. M. Furse, and Y. C. Chung, "Design of Implantable Microstrip Antenna for Communication with Medical Implants," *IEEE Transactions on Microwave Theory and Techniques*, **52**, 8, August 2004, pp. 1944-1951.

16. G. Kiziltas, D. Psychoudakis, J. L. Volakis, and N. Kikuchi, "Topology Design Optimization of Dielectric Substrates for Bandwidth Improvement of a Patch Antenna," *IEEE Transactions on Antennas and Propagation*, **AP-51**, 10, October 2003, pp. 2732-2743.

17. Y. Zhou, C. C. Chen, J. L. Volakis, "Dual Band Proximity-Fed Stacked Patch Antenna for Tri-Band GPS Applications," *IEEE Transactions on Antennas and Propagation*, **AP-55**, 1, January 2007, pp. 220-223.

18. T. Karacolak, A. Z. Hood, and E. Topsakal, "Design of a Dual-Band Implantable Antenna and Development of Skin Mimicking Gels for Continuous Glucose Monitoring," *IEEE Transactions on Microwave Theory and Techniques*, **56**, 4, April 2008, pp. 1001-1008.

19. R. Warty, M. R Tofighi, U. Kawoos, and A. Rosen, "Characterization of Implantable Antennas for Intracranial Pressure Monitoring: Reflection By and Transmission Through a Scalp Phantom," *IEEE Transactions on Microwave Theory and Techniques*, **56**, 10, October 2008, pp. 2366-2376.

20. T. Karacolak, R. Cooper, J. Butler, S. Fisher, and E. Topsakal, "In Vivo Verification of Implantable Antennas Using Rats as Model Animals," *IEEE Antennas and Wireless Propagation Letters*, **9**, 2010, pp. 334-337.

21. A. K. Skrivervik and F. Merli, "Design Strategies for Implantable Antennas," Proceedings of the Antennas and Propagation Conference, Loughborough, UK, November 2011.

22. J. Abadia, F. Merli, J. F. Zurcher, J. R. Mosig, and A. K. Skrivervik, "3D Spiral Small Antenna Design and Realization for Biomedical Telemetry in the MICS Band," *Radioengineering*, **18**, 4, December 2009, pp. 359-367.

23. C. Gabriel, S. Gabriel, and E. Corthout, "The Dielectric Properties of Biological Tissues: I. Literature Survey," *Physics in Medicine and Biology*, **41**, November 1996, pp. 2231-2249.

24. S. Gabriel, R. W. Lau, and C. Gabriel, "The Dielectric Properties of Biological Tissues: II. Measurements in the Frequency Range 10 Hz to 20 GHz," *Physics in Medicine and Biology*, **41**, November 1996, pp. 2251-2269.

25. S. Gabriel, R. W. Lau, and C. Gabriel, "The Dielectric Properties of Biological Tissues: III. Parametric Models for the Dielectric Spectrum of Tissues," *Physics in Medicine and Biology*, **41**, November 1996, pp. 2271-2293.

26. A. Kiourti, M. Christopoulou, and K. S. Nikita, "Performance of a Novel Miniature Antenna Implanted in the Human Head for Wireless Biotelemetry," IEEE International Symposium on Antennas and Propagation, Spokane, Washington, July 2011.

27. A. Kiourti and K. S. Nikita, "Miniature Scalp-Implantable Antennas for Telemetry in the MICS and ISM Bands: Design, Safety Considerations and Link Budget Analysis," *IEEE Transactions on Antennas and Propagation* (to appear).

28. A. Kiourti, M. Tsakalakis, and K. S. Nikita, "Parametric Study and Design of Implantable PIFAs for Wireless Biotelemetry," Proceedings of the 2nd ICST International Conference on Wireless Mobile Communication and Healthcare (MobiHealth 2012), Kos Island, Greece, October 2011.

29. A. Kiourti and K. S. Nikita, "Meandered Versus Spiral Novel Miniature PIFAs Implanted in the Human Head: Tuning and Performance," Proceedings of the 2nd ICST International Conference on Wireless Mobile Communication and Healthcare (MobiHealth 2012), Kos Island, Greece, October 2011.

30. P. Soontornpipit, C. M. Furse, and Y. C. Chung, "Miniaturized Biocompatible Microstrip Antenna Using Genetic Algorithm," *IEEE Transactions on Antennas and Propagation*, **AP-53**, 6, June 2005, pp. 1939-1945.

31. W. C. Liu, S. H. Chen, and C. M. Wu, "Implantable Broadband Circular Stacked PIFA Antenna for Biotelemetry Communication," *Journal of Electromagnetic Waves and Applications*, **22**, 13, 2008, pp. 1791-1800.

32. J. Kim and Y. Rahmat-Samii, "Implanted Antennas Inside a Human Body: Simulations, Designs, and Characterizations," *IEEE Transactions on Microwave Theory and Techniques*, **52**, 8, August 2004, pp. 1934-1943.

33. C. J. Sánchez-Fernández, O. Quevedo-Teruel, J. Requena-Carrión, L. Inclán-Sánchez, and E. Rajo-Iglesias, "Dual-Band Microstrip Patch Antenna Based on Short-Circuited Ring and Spiral Resonators for Implantable Medical Devices," *IET Microwaves Antennas and Propagation*, **4**, 8, August 2010, pp. 1048-1055.

34. J. Kim and Y. Rahmat-Samii, "SAR Reduction of Implanted Planar Inverted F Antennas with Non-Uniform Width Radiator," IEEE International Symposium on Antennas and Propagation, Albuquerque, New Mexico, July 2006.

35. J. Kim and Y. Rahmat-Samii, "Planar Inverted F Antennas on Implantable Medical Devices: Meandered Type Versus Spiral Type," *Microwave and Optical Technology Letters*, **48**, 3, March 1996, pp. 567-572.

36. W. Huang and A. A. Kishk, "Embedded Spiral Microstrip Implantable Antenna," *Hindawi International Journal of Antennas and Propagation*, **2011**, 2011, pp. 1-6.

37. C. M. Lee, T. C. Yo, F. J. Huang, and C. H. Luo, "Bandwidth Enhancement of Planar Inverted-F Antenna for Implantable Biotelemetry," *Microwave and Optical Technology Letters*, **51**, 3, March 2009, pp. 749-752.

38. C. M. Lee, T. C. Yo, and C. H. Luo, "Compact Broadband Stacked Implantable Antenna for Biotelemetry with Medical Devices," Proceedings of the IEEE Annual Conference on Wireless Microwave Technology (WAMICON 2006), Clearwater, Florida, December 2006.

39. H. Permana, Q. Fang, and I. Cosic, "3-Layer Implantable Microstrip Antenna Optimized for Retinal Prosthesis System in MICS band," Proceedings of the IEEE International Symposium on Bioelectronics and Bioinformatics (ISBB 2011), November 2011.

40. F. J. Huang, C. M. Lee, C. L. Chang, L. K. Chen, T. C. Yo, and C. H. Luo, "Rectenna Application of Miniaturized Implantable Antenna Design for Triple-Band Biotelemetry Communication," *IEEE Transactions on Antennas and Propagation*, **AP-59**, 7, July 2011, pp. 2646-2653.

41. W. C. Liu, F. M. Yeh, and M. Ghavami, "Miniaturized Implantable Broadband Antenna for Biotelemetry Communication," *Microwave and Optical Technology Letters*, **50**, 9, September 2008, pp. 2407-2409.

42. W. C. Liu, S. H. Chen, and C. M. Wu, "Bandwidth Enhancement and Size Reduction of an Implantable PIFA Antenna for Biotelemetry Devices," *Microwave and Optical Technology Letters*, **51**, 3, March 2009, pp.755-757.

43. IEEE Standard for Safety Levels with Respect to Human Exposure to Radiofrequency Electromagnetic Fields, 3 kHz to 300GHz, IEEE Standard C95.1, 1999.

44. International Commission on Non-Ionizing Radiation Protection, "Guidelines for Limiting Exposure to Time-Varying Electric, Magnetic, and Electromagnetic Fields (up to 300 GHz)," *Health Physics*, **74**, 1998, pp. 494-522.

45. IEEE Standard for Safety Levels with Respect to Human Exposure to Radiofrequency Electromagnetic Fields, 3 kHz to 300 GHz, IEEE Standard C95.1, 2005.

46. Medical Implantable RF Transceiver ZL70101 Data Sheet Zarlink Semiconductor, Ottawa, ON, Canada, October 2006.

47. Z. Noroozi, and F. Hojjat-Kashani, "Three-Dimensional FDTD Analysis of the Dual-Band Implantable Antenna for Continuous Glucose Monitoring," *Progress in Electromagnetics Research Letters*, **28**, 2012, pp. 9-21.

48. D. Rucker, A. Al-Alawi, R. Adada, and H. M. Al-Rizzo, "A Miniaturized Tunable Microstrip Antenna for Wireless Communications with Implanted Medical Devices," Proceedings of the 2nd International ICST Conference on Body Area Networks (BodyNets 2007), Brussels, Belgium, June 2007.

49. F. Merli and A. K. Skrivervik, "Design and Measurement Considerations for Implantable Antennas for Telemetry Applications," Proceedings of the 4th European Conference on Antennas and Propagation (EuCAP 2010), Barcelona, Spain, April 2010.

50. T. Karacolak, R. Cooper, and E. Topsakal, "Electrical Properties of Rat Skin and Design of Implantable Antennas for Medical Wireless Telemetry," *IEEE Transactions on Antennas and Propagation*, **57**, 9, September 2009, pp. 2806-2812.

51. A. Sani, M. Rajab, R. Foster, and Y. Hao, "Antennas and Propagation of Implanted RFIDs for Pervasive Healthcare Applications," *Proceedings of the IEEE*, **98**, 9, September 2010, pp. 1648-1655.

52. R. Zajicek, L. Oppl, and J. Vrbaf, "Broadband Measurement of Complex Permittivity Using Reflection Method and Coaxial Probes," *Radioengineering*, **17**, April 2008, pp. 14-19.

53. U. Kawoos, M. R. Tofighi, R. Warty, F. A Kralick, and A. Rosen, "In-Vitro and In-Vivo Trans-Scalp Evaluation of an Intracranial Pressure Implant at 2.4 GHz," *IEEE Transactions on Microwave Theory and Techniques*, **56**, 10, October 2008, pp. 2356-2365.

Introducing the Authors

Asimina Kiourti received the Diploma in Electrical and Computer Engineering from the University of Patras, Greece (2008), and the MSc in Technologies for Broadband Communications from University College London, UK (2009). In October 2009, she joined the Biomedical Simulations and Imaging Laboratory, National Technical University of Athens, where she is currently working towards her PhD. She has authored or coauthored one book chapter and 13 journal and conference papers. Her current research interests include antenna theory, medical telemetry, electromagnetics, and wireless communications.

Ms. Kiourti has received various awards and scholarships, among which are the IEEE MTT-S Graduate Fellowship for Medical Applications for 2012, and the IEEE AP-S Doctoral Research Award for 2011. She is a reviewer for the *IEEE Antennas and Wireless Propagation Letters* and the *IEEE Antennas and Propagation Magazine*. She has served on the organizing committee of three international conferences. She is a member of the Technical Chamber of Greece.

Konstantina S. Nikita received the Diploma in Electrical Engineering and a PhD from the National Technical University of Athens (NTUA), as well as the MD degree from the Medical School, University of Athens. From 1990 to 1996, she worked as a Researcher at the Institute of Communication and Computer Systems. In 1996, she joined the School of Electrical and Computer Engineering, NTUA, as an Assistant Professor, and since 2005 she has served as a Professor at the same school. She has authored or co-authored 160 papers in refereed international journals and chapters in books, and over 280 papers in international conference proceedings. She is editor or co-editor of two books in English, and author of two books in Greek. She holds two patents. She has been the technical manager of several European and National R&D projects. She has been honorary chair or chair of the program or organizing committees of several international conferences. She has served as a keynote or invited speaker at international conferences, symposia, and workshops organized by NATO, WHO, ICNIRP, IEEE, URSI, COMCON, PIERS, etc. She has been the advisor for 20 completed PhD theses, several of which have received various awards. Her current research interests include biomedical signal and image processing and analysis, biomedical informatics, simulation of physiological systems, medical imaging, biological effects and medical applications of radiofrequency electromagnetic fields.

Dr. Nikita is a member of the editorial board of the *IEEE Transactions on Biomedical Engineering*, and has been a guest editor of several international journals. She has received various honors and awards, among which is the prestigious Bodossakis Foundation Academic Prize for exceptional achievements in "Theory and Applications of Information Technology in Medicine" (2003). She has been a member of the Board of Directors of the Hellenic National Academic Recognition and Information Center and of the Greek Atomic Energy Commission, and a member of the Hellenic National Council of Research and Technology. She is a Fellow of the EAMBES, a member of the Technical Chamber of Greece, and a member of the Athens Medical Association. She is also the founding Chair and Ambassador of the IEEE-EMBS, Greece Chapter; Vice Chair of the IEEE Greece Section; and deputy Head of the School of Electrical and Computer Engineering of the NTUA.